Journal Name

RSC Publishing

COMMUNICATION

Targeted fluorescence imaging enhanced by 2D materials: A comparison between 2D MoS_2 and graphene oxide

ttCite this: DOI: 10.1039/x0xx00000x

Received 00th January 2016,
Accepted 00th January 2016

DOI: 10.1039/x0xx00000x

www.rsc.org/

Donghao Xie,[a1] Ding-Kun Ji,[b1] Yue Zhang,[bc] Jun Cao,[a] Hu Zheng,[a] Lin Liu,[a] Yi Zang,[c] Jia Li,[c]* Guo-Rong Chen,[b] Tony D James[d]* and Xiao-Peng He[b]*

Here we demonstrate that 2D MoS_2 can enhance the receptor-targeting and imaging ability of a fluorophore-labelled ligand. The 2D MoS_2 has an enhanced working concentration range when compared with graphene oxide, resulting in the improved imaging of both cell and tissue samples.

Receptor proteins are a class of important transmembrane biomacromolecules that control a diverse range of physiological processes. While a number of selective receptor-ligand interactions are key to the initiation of downstream cellular pathways, many other types of receptors are responsible for the endocytosis, and thus clearance, of harmful molecules from the circulation in blood. Some receptor proteins located on the surface of cells can facilitate the invasion of pathogens, however.[1] Recent studies have revealed an upregulation of carbohydrate receptors during inflammation and cancer metastasis.[2] As a result, receptor proteins are promising biomarkers for targeted disease diagnosis and therapy.[3-7]

Since the discovery of graphene which has demonstrated exceptional mechanical, optical and electrical properties, increasing efforts have been directed to the development of two-dimensional (2D) graphene analogues for application in a variety of research areas.[8-12] In particular, recent literature has seen an extensive interest in the construction of diagnostic and therapeutic materials based on 2D transition metal dichalcogenides (TMDs).[8-19] Compared to GO, the 2D TMDs are structurally more diverse, and some materials have proven to have a better biocompatibility for biological applications.[11-13]

The 2D TMDs can be easily functionalized with a diverse range of biomolecules and drugs by supramolecular assembly for biosensing and cancer therapy.[14-16] Owing to their intrinsic photothermal and photoacoustic properties, these TMDs have also been used for *in vivo* cancer theranostics.[17-19] While these pioneering investigations have highlighted the promise of TMDs as a new generation of biomedical tools, evidence for the applicability of TMDs to targeted bio imaging has been elusive.

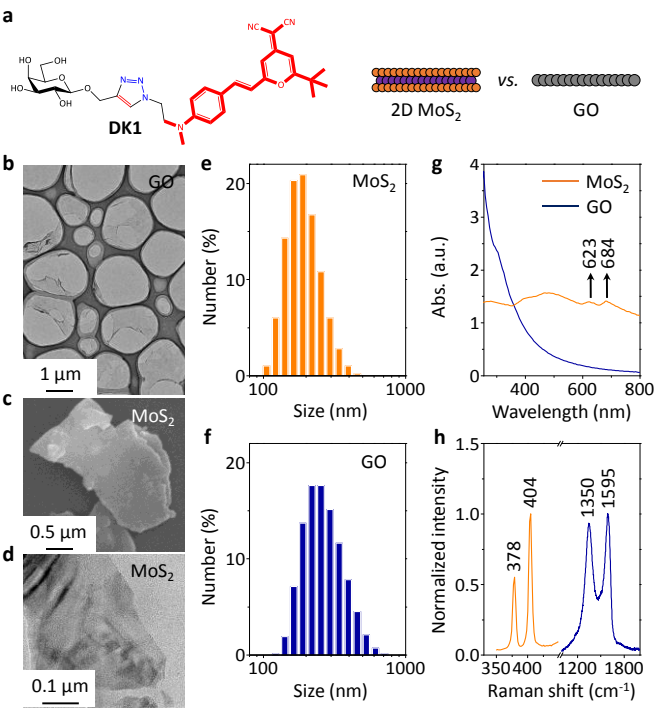

Figure 1. (a) Structure of the fluorophore-tagged glycoligand (**DK1**) and cartoon of 2D MoS_2 and graphene oxide (GO). High-resolution transmission electron microscopy of (b) GO and (d) 2D MoS_2. (c) Scanning electron microscopy of 2D MoS_2. Dynamic light scattering of (e) 2D MoS_2 and (f) GO. (g) Stacked UV-vis spectra of 2D MoS_2 and GO. (h) Stacked Raman spectra of 2D MoS_2 and GO.

Here, we report an interesting observation that a 2D TMD (molybdenum disulfide, MoS_2) drastically enhances the receptor-targeting and imaging ability of a fluorophore-labelled

ligand. The 2D MoS_2 shows a much better working concentration range than GO, improving the imaging for both cellular and tissue samples. As shown in Fig. 1a, we used the glycoligand (galactose) for, the asialoglycoprotein carbohydrate receptor (ASGPr).[20] The glycoligand was coupled to a red-emitting dicyanomethylene-4*H*-pyran (DCM) fluorescent dye by an efficient click reaction, producing glycoprobe (**DK1**) capable of cellular imaging (Fig. 1a).[21,22] Then, the receptor-targeting imaging ability of **DK1** was investigated using both 2D MoS_2 and GO (Fig. 1a).

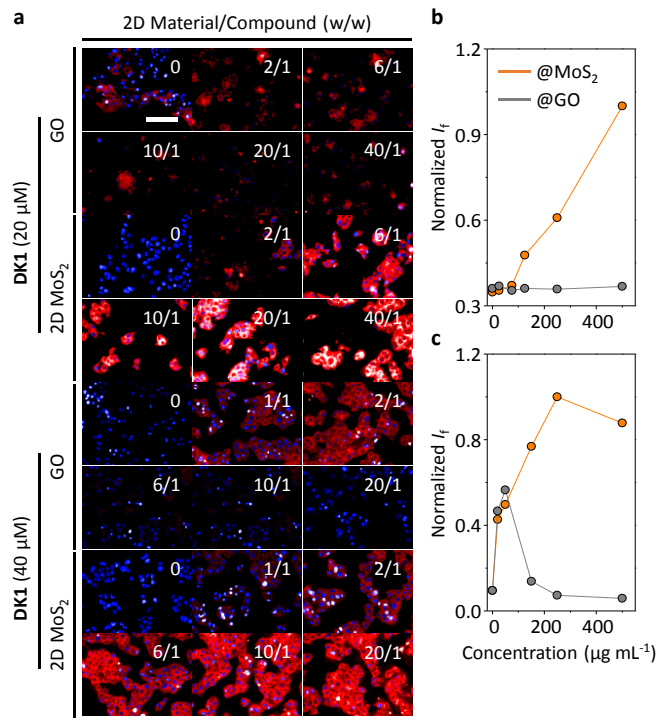

Figure 2. (a) Fluorescence imaging of Hep-G2 (human liver cancer) cells with **DK1** at two concentrations and fluorescence quantification of the cells with (b) 20 μM **DK1** and (c) 40 μM **DK1** in the absence and presence of increasing 2D MoS_2 or graphene oxide (GO). Scale bar = 100 μm (applicable to all images). Exitation channel: 520-550 nm; emission: 580-650 nm.

GO was produced using the modified Hummer's method,[5] and 2D MoS_2 was prepared using the recently established, simple liquid exfoliation method from commercial MoS_2 powder.[23] The resulting 2D materials were characterized by a series of microscopic and spectroscopic techniques (Fig. 1). Fig 1b, Fig. 1c and Fig. 1d show the high-resolution transmission electron microscope (HRTEM) image of GO, scanning electron microscope (SEM) image of 2D MoS_2 and TEM image of 2D MoS_2, respectively. The objects observed in these images appear to be thin flakes. Dynamic light scattering (DLS) suggested a similar size distribution for the 2D MoS_2 (Fig. 1e) and GO (Fig. 1f) sheets. Moreover, typical UV-vis and Raman peaks were observed for both materials. While a characteristic broad UV absorbance band for GO was observed,[24,25] and typical absorbance peaks at 623 and 684 nm, assigned to the A1 and B1 direct exciton transitions of 2D MoS_2, respectively, were observed.[26-28] The typical D band (1350 cm^{-1}) and G band (1595 cm^{-1}) indicated the presence of GO sheets,[5] whereas peaks centered at 404 and 378 cm^{-1}, which are the A_{1g} (out-of-plane vibration of S) and E^1_{2g} (in-plane relative motion between S and Mo) modes of hexagonal MoS_2, respectively, suggest the formation of 2D MoS_2.[29] In addition, the materials were also characterized using Zeta potential analysis (Fig. S1) and fluorescence spectroscopy (Fig. S2). The results indicate a negatively charged nature[30,31] and weak intrinsic fluorescence emission of the 2D materials.

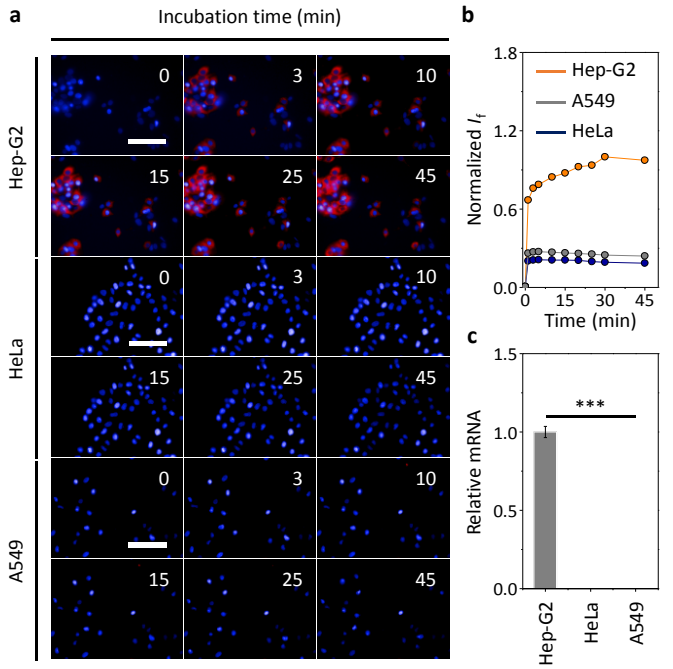

Figure 3. Fluorescence imaging (a) and quantification (b) of Hep-G2 (human liver cancer), HeLa (human cervix cancer) and A549 (human lung cancer) cells with 10 μM **DK1** in the absence of 62.5 μg mL^{-1} 2D MoS_2. (c) Relative mRNA level of different cells determined by real-time quantitative polymerase chain reaction (***P<0.001; n. d. = not detectable). Scale bar = 100 μm (applicable to all images). Exitation channel: 520-550 nm; emission: 580-650 nm.

With the fluorophore-labelled ligand and the 2D materials in hand, we performed cellular imaging assays. **DK1** (at two different concentrations) with or without increasing amounts of 2D MoS_2 or GO were incubated with Hep-G2 (human liver cancer) cells that significantly express ASGPr[20] for 15 min. Subsequently fluorescence images were recorded and the fluorescence intensities quantified (Fig. 2). As shown in Fig. 2a, while the fluorescence imaging effect of the **DK1** alone was weak for Hep-G2, the presence of increasing 2D MoS_2 drastically increased the fluorescence. We also observed that the presence of increasing GO did not enhance the fluorescence under similar imaging conditions. To quantify these results, the fluorescence intensities of the cell lines were measured (Fig. 2b and Fig. 2c). Similarly, the result indicate that the presence of increasing 2D MoS_2 enhances the fluorescence of the cell lines (except for 40 μM **DK1** with 500 μg mL^{-1} 2D MoS_2, Fig. 2c). In contrast, the presence of increasing GO did not enhance the fluorescence. The only exception is the mixture of 40 μM **DK1** with a small amount of GO (25 μg mL^{-1} and 50 μg mL^{-1}).[32] However, further increase of the GO concentration led to sharp fluorescence

quenching. This result suggests a better working concentration range for 2D MoS_2 than GO.

To test whether the fluorescence imaging is predominantly based on ASGPr-glycoligand interactions, we used a cervical cancer cell line (HeLa) and a lung cancer cell line (A549) without ASGPr expression as control.[33-35] From both fluorescence imaging (Fig. 3a) and quantification (Fig. 3b) we determined that the fluorescence for both cells quickly reached equilibrium. Interestingly, over the whole time period, the material produced a stronger fluorescence with Hep-G2 than with HeLa and A549, suggesting that the enhancement was caused by ligand-ASGPr recognition events. Notably, the fluorescence imaging results were in good agreement with the ASGPr expression level of the cells, as determined by real-time quantitative polymerase chain reaction (RT-qPCR) (Fig. 3c).

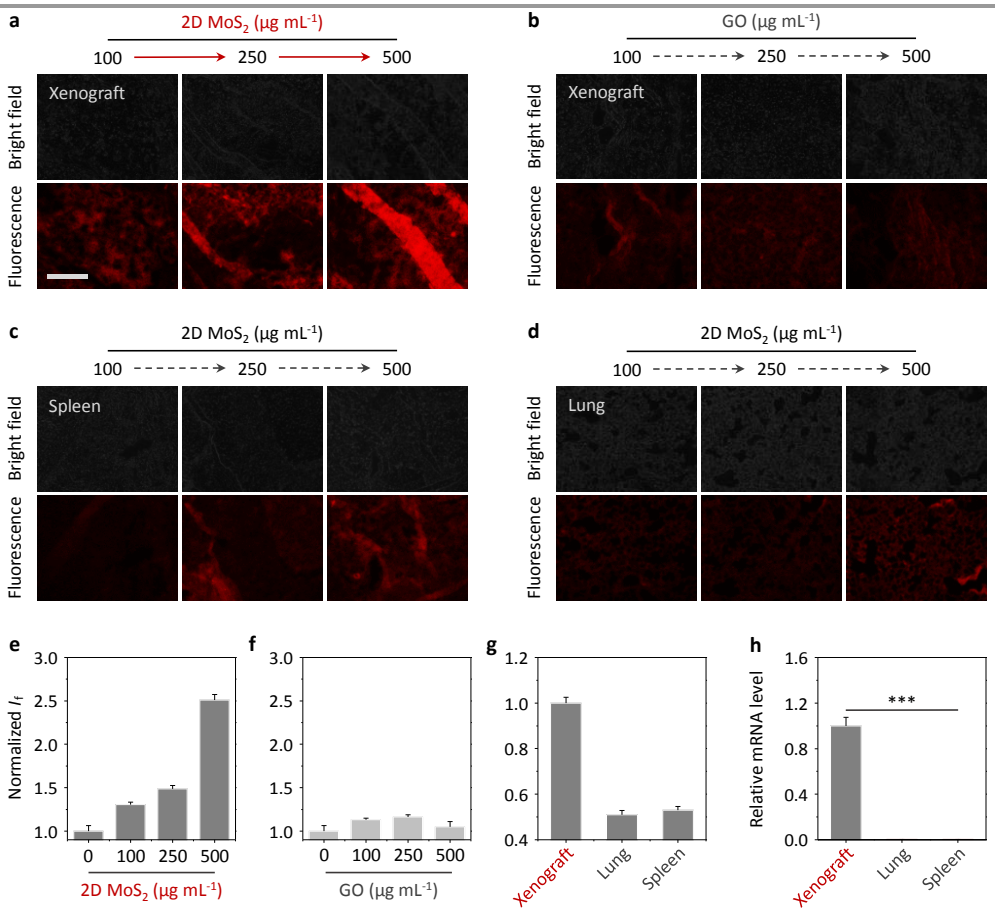

Figure 4. Fluorescence imaging of (a) xenograft section with 10 μM **DK1** in the presence of increasing 2D MoS_2, (b) xenograft section with 10 μM **DK1** in the presence of increasing GO, (c) spleen section with 10 μM **DK1** in the presence of increasing 2D MoS_2 and (d) lung section with 10 μM **DK1** in the presence of increasing 2D MoS_2. Fluorescence quantification of (e) xenograft section with 10 μM **DK1** in the presence of increasing 2D MoS_2, (f) xenograft section with 10 μM **DK1** in the presence of increasing GO and (g) different tissue sections in the presence of 500 μg mL^{-1} 2D MoS_2. (h) Relative mRNA level of different tissue sections determined by real-time quantitative polymerase chain reaction (*** P<0.001). Scale bar = 100 μm (applicable to all images). Exitation channel: 520-550 nm; emission: 580-650 nm.

Subsequently, we used tissue samples to investigate the imaging properties of the 2D materials. A female athymic BALB/c nu/nu mouse with a Hep-G2-bearing xenograft was used.[32] The collected tissue sections were the xenograft and two healthy organs, the spleen and the lung. We determined that with an increasing concentration of 2D materials, the fluorescence of **DK1** gradually increased with xenograft section in the presence of 2D MoS_2 (Fig. 4a and Fig. 4e), but not for GO (Fig. 4b and Fig. 4f). In addition, a fluorescence increase was not observed for the spleen (Fig. 4c and Fig. 4g) or lung sections (Fig. 4d and Fig. 4g), which were shown to hardly express ASGPr by RT-qPCR (Fig. 4h).

In summary, we have demonstrated that 2D MoS_2 can significantly enhance the fluorescence imaging ability of fluorophore-labelled ligand molecules for transmembrane receptors in a concentration dependent manner. Compared to GO, a 2D carbon material widely used for biosensing and bioimaging, the working concentration range for the 2D MoS_2 was significantly improved. This research suggests that 2D materials with similar morphology but different chemical components might function differently at certain cellular interfaces. This study may also provide insight into the development of other effective low-dimensional materials for targeted theranostics.[36-39]

This research is supported by the 973 project (2013CB733700), the National Natural Science Foundation of China (21572058 and 21576088), the Shanghai Health and Family Planning Commission Research Fund (201540158), the Science and Technology

Commission of Shanghai Municipality (15540723800) and the Shanghai Rising-Star Program (16QA1401400). Prof. Xiongwen Zhang at ECNU is warmly thanked for kindly gifting the xenograft mice. The Catalysis And Sensing for our Environment (CASE) network is thanked for research exchange opportunities. T.D.J. thanks ECUST for a guest professorship.

Notes and references

[a] Department of Pharmacy & Department of Interventional Oncology, Dahua Hospital, Xuhui District, Shanghai, 200237, PR China

[b] Key Laboratory for Advanced Materials & Institute of Fine Chemicals, School of Chemistry and Molecular Engineering, East China University of Science and Technology, Shanghai 200237, PR China. Email: xphe@ecust.edu.cn

[c] National Center for Drug Screening, State Key Laboratory of Drug Research, Shanghai Institute of Materia Medica, Chinese Academy of Sciences, 189 Guo Shoujing Rd., Shanghai 201203, PR China. Email: jli@simm.ac.cn

[d] Department of Chemistry, University of Bath, Bath, BA2 7AY, UK. Email: t.d.james@bath.ac.uk

[1]Equal contribution

Electronic Supplementary Information (ESI) available: [Additional figures and experimental section]. See DOI: 10.1039/c000000x/

1 R. Xu, R. P. de Vires, X. Zhu, C. M. Nycholat, R. McBribe, W. Yu, J. C. Paulson and I. A. Wilson, *Science*, 2013, **342**, 1230.
2 T. Lawrence and G. Natoli, *Nat. Rev. Immunol.*, 2011, **11**, 750.
3 E. I. Rigopoulou, D. Roggenbuck, D. S. Smyk, C. Liaskos, M. G. Mythilinaiou, E. Feist, K. Conrad, and D. P. Bogdanos, *Autoimmun. Rev.*, 2012, **12**, 260.
4 K. Jain, P. Kesharwani, U. Gupta, and N. K. Jain, *Biomaterials*, 2012, **33**, 4166.
5 H.-L. Zhang, X.-L. Wei, Y. Zang, J.-Y. Cao, S. Liu, X.-P. He, Q. Chen, Y.-T. Long, J. Li, G.-R. Chen and K. Chen, *Adv. Mater.*, 2013, **25**, 4097.
6 W. Ma, H.-T. Liu, X.-P. He, Y. Zang, J. Li, G.-R. Chen, H. Tian and Y.-T Long, *Anal. Chem.*, 2014, **86**, 5502.
7 X.-P. He, B.-W. Zhu, Y. Zang, J. Li, G.-R. Chen, H. Tian and Y.-T. Long, *Chem. Sci.*, 2015, **6**, 1996.
8 Q. H. Wang, K. Kalantar-Zadeh, A. Kis, J. N. Coleman and M. S. Strano, *Nat. Nanotechnology*, 2012, **7**, 699.
9 M.-R. Gao, Y.-F. Xu, J. Jiang and S.-H. Yu, *Chem. Soc. Rev.*, 2013, **42**, 2986.
10 H. Wang, H. Feng and J. Li, *Small*, 2014, **10**, 2165.
11 M. Pumera and A. H. Loo, *Trends Anal. Chem.*, 2014, **61**, 49.
12 Y. Chen, C. Tan, H. Zhang and L. Wang, *Chem. Soc. Rev.*, 2015, **44**, 2681.
13 W. Z. Teo, E. L. K. Chng, Z. Sofer and M. Pumera, *Chem. Eur. J.*, 2014, **20**, 9627.
14 C. Zhu, Z. Zeng, H. Li, F. Li, C. Fan and H. Zhang, *J. Am. Chem. Soc.*, 2013, **135**, 5998.
15 Y. Zhang, B. Zheng, C. Zhu, X. Zhang, C. Tan, H. Li, B. Chen, J. Yang, J. Chen, Y. Huang, L. Wang and H. Zhang, *Adv. Mater.*, 2015, **27**, 935.
16 H. Fan, Z. Zhao, G. Yan, X. Zhang, C. Yang, H. Meng, Z. Chen, H. Liu and W. Tan, *Angew. Chem. Int. Ed.*, 2015, **54**, 4801.
17 L. Cheng, J. Liu, X. Gu, H. Gong, X. Shi, T. Liu, C. Wang, X. Wang, G. Liu, H. Xing, W. Bu, B. Sun and Z. Liu, *Adv. Mater.*, 2014, **26**, 1886.
18 T. Liu, C. Wang, X. Gu, H. Gong, L. Cheng, X. Shi, L. Feng, B. Sun and Z. Liu, *Adv. Mater.*, 2014, **26**, 3433.
19 S. S. Chou, B. Kaehr, J. Kim, B. M. Foley, M. De, P. E. Hopkins, J. Huang, C. J. Brinker and V. P. Dravid, *Angew. Chem. Int. Ed.*, 2013, **52**, 4160.
20 J. B. Burgess, J. U. Baenziger and W. R. Brown, *Hepatology*, 1992, **15**, 702.
21 D.-K. Ji, G.-R. Chen, X.-P. He and H. Tian. *Adv. Funct. Mater.*, 2015, **25**, 3483.
22 D.-K. Ji, Y. Zhang, X.-P. He and G.-R. Chen, *J. Mater. Chem. B*, 2015, **3**, 6656.
23 J. N. Coleman, M. Lotya, A. O'Neill, S. D. Bergin, P. J. King, K. Young, A. Gaucher, S. De, R. J. Smith, I. V. Shvets, S. K. Arora, G. Stanton, H.-Y. Kim, K. Lee, G. T. Kim, G. S. Duesberg, T. Hallam, J. J. Boland, J. J. Wang, J. F. Donegan, J. C. Grunlan, G. Moriarty, A. Shmeliov, R. J. Nicholls, J. M. Perkins, E. M. Grieveson, K. Theuwissen, D. W. McComb, P. D. Nellist and V. Nicolosi, *Science*, 2011, **311**, 568.
24 L. Feng, L. Wu and X. Qu, *Adv. Mater.*, 2013, **25**, 168.
25 E. Morales-Narváez and A. Merkoçi, *Adv. Mater.*, 2012, **24**, 3298.
26 P. T. K. Loan, W. Zhang, C.-T. Lin, K.-H. Wei, L.-J. Li and C.-H. Chen, *Adv. Mater.*, 2014, **26**, 4838.
27 H. Li, G. Lu, Z. Yin, Q. He, H. Li, Q. Zhang and H. Zhang, *Small*, 2012, **8**, 682.
28 L. Su, Y. Zhang, Y. Yu and L. Cao, *Nanoscale*, 2014, **6**, 4920.
29 Y. Yang, T. Liu, L. Cheng, G. Song, Z. Liu and M. Chen, *ACS Appl. Mater. Interfaces*, 2015, **7**, 7526.
30 D. Li, M. B. Muller, S. Gilje, R. B. Kaner and G. G. Wallace, *Nat. Nanotechnol.*, 2008, **3**, 101.
31 K.-G. Zhou, N.-N. Gao, H.-X. Wang, Y. Peng and H.-L. Zhang, *Angew. Chem. Int. Ed.*, 2011, **50**, 10839.
32 D.-K. Ji, Y. Zhang, Y. Zang, W. Liu, X. Zhang, J. Li, G.-R. Chen, T. D. James and X.-P. He, *J. Mater. Chem. B*, 2015, **3**, 9182.
33 K.-B. Li, Y. Zang, H. Wang, J. Li, G.-R. Chen, T. D. James, X.-P. He and H. Tian, *Chem. Commun.*, 2014, **50**, 11735.
34 L. Dong, Y. Zang, D. Zhou, X.-P. He, G.-R. Chen, T. D. James and J. Li, *Chem. Commun.*, 2015, **51**, 11852.
35 D.-T. Shi, D. Zhou, Y. Zang, J. Li, G.-R. Chen, T. D. James, X.-P. He and H. Tian, *Chem. Commun.,* 2015, **51**, 3653.
36 X.-P. He and H. Tian, *Small*, 2016, **12**, 144.
37 D. Chimene, D. L. Alge and A. K. Gaharwar, *Adv. Mater.*, 2015, **27**, 7261.
38 X.-L. Hu, Y. Zang, J. Li, G.-R. Chen, T. D. James, X.-P. He and H. Tian, *Chem. Sci.*, 2016, **7**, 4004.
39 X.-P. He, Y.-L. Zeng, Y. Zang, J. Li, R. A. Field and G.-R. Chen, *Carbohydr. Res.*, 2016, **429**, 1.

